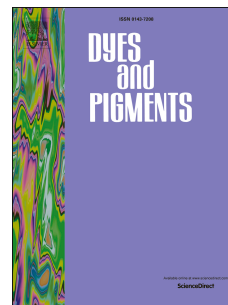# Journal Pre-proof

Preparation and luminescence properties of isoquinoline-nucleated polycyclic aromatics

Yanmei Li, Xinyu Li, Tianzhi Yu, Wenming Su, Youjia Wang, Yuling Zhao, Hui Zhang

Please cite this article as: Li Y, Li X, Yu T, Su W, Wang Y, Zhao Y, Zhang H, Preparation and luminescence properties of isoquinoline-nucleated polycyclic aromatics, *Dyes and Pigments* (2019), doi: https://doi.org/10.1016/j.dyepig.2019.107803.

This is a PDF file of an article that has undergone enhancements after acceptance, such as the addition of a cover page and metadata, and formatting for readability, but it is not yet the definitive version of record. This version will undergo additional copyediting, typesetting and review before it is published in its final form, but we are providing this version to give early visibility of the article. Please note that, during the production process, errors may be discovered which could affect the content, and all legal disclaimers that apply to the journal pertain.

Graphical Abstract:

Preparation and luminescence properties of isoquinoline-nucleated polycyclic aromatics

Yanmei Li‡[1], Xinyu Li‡[1], Tianzhi Yu[1,*], Wenming Su[2,*], Youjia Wang[1], Yuling Zhao[3], Hui Zhang[1]

[1]Key Laboratory of Opto-Electronic Technology and Intelligent Control (Ministry of Education), Lanzhou Jiaotong University, Lanzhou 730070, China

[2]Printable electronics research center, Suzhou Institute of Nano-Tech and Nano-Bionics, Chinese Academy of Sciences, Suzhou 215123, China

[3]School of Chemical and Biological Engineering, Lanzhou Jiaotong University, Lanzhou 730070, China

Abstract: Two isoquinoline-nucleated polycyclic aromatic compounds, 4,5-diphenyl-7*H*-dibenzo[*de*,*g*]quinolin-7-one (**A**) and 3,4-diphenyl-6*H*-phenanthro[3,4,5-*defg*]quinolin-6-one (**B**), were synthesized in high yields through three-component reaction of phenanthrene diketone or pyrene diketone, ammonium acetate and 1,2-diphenylethyne in one-pot. Their structures, thermal stabilities, photophysical properties and energy levels are investigated systematically. Both compounds emit very weak fluorescence in acetone, but their luminescence intensity increased significantly when the water content reaches 50% for **A** and 40% for **B**, exhibiting aggregation-induced emission (AIE) characteristics, and showing that the AIE effect of the compound **A** is stronger than that of the compound **B**. The vacuum-processed doped devices based on the compound **B** showed green

---

* Corresponding Authors.

  Tianzhi Yu, E-mail: yutzh@mail.lzjtu.cn; Wenming Su, E-mail: wmsu2008@sinano.ac.cn

  ‡These authors are contributed equally

emission with a maximum brightness of 2162 cd/m^2, a maximum current efficiency of 2.97 cd/A and a maximum external quantum efficiency (EQE) of 2.23%.

Key words: Polycyclic aromatic compound; Alkyne annulation; Aggregation-induced emission (AIE); Photoluminescence; Electroluminescence

1. Introduction

Polycyclic aromatic hydrocarbons (PAHs), such as anthracen, pyrene and perylene, have been used widespreadly in molecular electronics, optoelectronics, energy conversion devices and various other forms of nanotechnology due to their chemical stabilities and photochemical properties [1-6]. Due to the high abilities of fluorescence and charge-transport, PAHs are widely used as the building blocks for molecular materials for organic electronics [7-11]. Recently, numerous heteroaromatic ring fused PAHs exhibit fundamentally interesting and even practically useful electrochemical and photophysical properties as the components of organic electronic devises [12-16]. Therefore, the synthesis and structural elucidation of heteroaromatic ring fused PAHs are of high interest [17-22].

Transition metal-catalyzed activation and functionalization of normally unreactive C–H bonds have become an increasingly efficient and reliable approach for new carbon–carbon and carbon–heteroatom bond formations [23-26], which allows the use of less expensive and more readily available starting materials to obtain complex compounds in an atom- and step-economic way. Since Murai and coworkers first reported on ruthenium(0)-catalyzed addition of aromatic C–H bonds to alkenes [27], various transition metal complexes have been employed as catalysts for C–H bond functionalization to produce a variety of heterocycles over the past decades. Among the

2

transition metal catalysts, the oxidative cyclization reactions of the alkenes and alkynes by utilizing the less expensive and stable rhodium (III) complex $[Cp*RhCl_2]_2$ were proved to be a fast access to heterocycles due to the high efficiency, selectivity and functional group tolerance [25]. In the past few years, the $[Cp*RhCl_2]_2$-catalyzed annulation of various aromatic substrates with alkynes using $Cu(OAc)_2 \cdot H_2O$ as the oxidant was extensively used in the synthesis of heterocyclic compounds. For example, the treatment of the substituted aromatic acids with alkynes using $[Cp*RhCl_2]_2$ and $Cu(OAc)_2 \cdot H_2O$ in o-xylene or DMF under N_2 can afford various isocoumarin products in good yields [28]. In the presence of $Co(OAc)_2 \cdot 4H_2O$ as the co-catalyst, Wang et al. [29] synthesized a series of naphtho[1′,2′:4,5]imidazo[1,2-a]pyridines from 2-arylimidazo[1,2-a]pyridines and alkynes via Rh-catalyzed ($[Cp*RhCl_2]_2$) double C-H activation, in which some products exhibited deep blue emissions. The Hua group reported an efficient method for the synthesis of ring-fused and π-extended phenanthroimidazoles from one-pot four-component reaction of 9,10-phenanthraquinone, ammonium acetate, aldehydes and alkynes using $[Cp*RhCl_2]_2$ catalyst associated with the oxidant $Cu(OAc)_2 \cdot H_2O$ in trifluoroethanol (TFE) [30]. Recently, our group also reported two luminescent phenanthroimidazoisoquinoline derivatives via facile multicomponent reaction in one-pot [12].

For some π–conjugated planar organic compounds, they exhibit strong emission in the dilute solutions, but their fluorescence is weakened or even quenched in the concentrated solution and solid state due to the concentration-quenching effect (CQE) or the aggregation-caused quenching (ACQ) caused by the strong intermolecular π–π stacking interactions between neighboring fluorophores [31,32]. The CQE and ACQ phenomena of luminophores in the concentrated solutions and solid states drastically limit their practical applications as fluorescence sensors, biological

probes, polarized light emitters, emitting materials in organic light-emitting diodes (OLEDs), etc. Although introduction of bulky substituents into molecular structures of the luminophores can help change luminophores from being weakly luminescent to strongly emissive in the solid state [33-35], this strategy can not fundamentally solve the CQE and ACQ effects because the aggregate formation is an intrinsic process for luminogenic molecules in the condensed phase. In 2001, Tang group first discovered the aggregation-induced emission (AIE) phenomenon that some fluorophores were non-emissive in dilute solutions but became highly luminescent in concentrated solutions or in solid films [36,37]. So far several kinds of luminescent materials with AIE effect have been synthesized and successfully applied in OLEDs, probes and optical memory materials [38-43].

As a part of our continuous researches in developing new luminescent polycyclic aromatic hydrocarbons (PAHs) for OLEDs, in this study, two new isoquinoline-nucleated polycyclic aromatics with AIE effect were synthesized by one-pot method. Their photophysical and AIE properties and thermal stability of the compounds were investigated. In addition, the investigation of the vacuum-processed OLED devices and performances using the compounds as emitting materials were also reported.

2. Experimental

2.1 Materials and methods

Phenanthrene-9,10-dione, pyrene, *N*-methylimidazole (NMI), $NaIO_3$, $RuCl_3 \cdot 3H_2O$, 1,2-diphenylacetylene and 2,2,2-trifluoroethanol (TFE) were obtained from Energy Chemical (China). Bis[(pentamethylcyclopentadienyl)dichloro-rhodium] ($[Cp^*RhCl_2]_2$) was purchased from Beijing HWRK Chem. Co. LTD (China). All the other chemicals were analytical grade reagent.

Toluene was dried over sodium and freshly distilled prior in the related reaction.

^{1}H and ^{13}C NMR spectra were recorded on Bruker 500, AVANCE NEO. Mass spectra were recorded using a Thermo Scientific Orbitrap Elite mass spectrometer. C, H, and N analyses were obtained using an Elemental Vario-EL automatic elemental analysis instrument. Thermogravimetric analysis (TGA) was performed on a PerkinElmer Pyris system. UV-vis absorption spectra were recorded on a Shimadzu UV-2550 spectrometer. The cyclic voltammograms were performed on a electrochemical analyzer (CHI Instruments 760 B). The photoluminescence quantum yield was measured by an absolute method using the Edinburgh Instruments FLS920 integrating sphere with the Xe lamp at room temperature. The photoluminescence decay lifetime was measured by a time-correlated single photon counting spectrometer using Edinburgh Instruments FLS920 with a microsecond flashlamp as the excitation source (repetition rate 90 Hz) at room temperature.

2.2 Synthesis and characterization of the 4,5-diphenyl-7H-dibenzo[de,g]quinolin-7-one (A) and 3,4-diphenyl-6H-phenanthro[3,4,5-$defg$]quinolin-6-one (B)

Pyrene-4,5-dione: The intermediate pyrene-4,5-dione was prepared according to the literature [44]. Pyrene (5.00 g, 24.72 mmol), NMI (0.10 g, 1.22 mmol) and RuCl$_3$•3H$_2$O (0.65 g, 2.49 mmol) were dissolved in the mixed solvent of DCM (100 mL), THF (100 mL) and H$_2$O (125 mL). Then, NaIO$_4$ (23.80 g, 111.27 mmol) was added in small portions over 5 min. The reaction mixture was stirred for 2 h under a nitrogen atmosphere. The resulting mixture was poured into 200 mL of water and extracted with dichloromethane (3 × 100 mL). The organic phase was washed with water (2 × 100mL) and dried over anhydrous Na$_2$SO$_4$. After filtration and evaporation of the solvent in vacuum, the crude was purified by chromatography on silica gel

using dichloromethane/petroleum ether (1:5, v/v) as the eluent to obtain pyrene-4,5-dione (2.81 g, 48.95%). ^{1}H NMR (500 MHz, CDCl$_3$, δ): 8.50 (d, J = 7.4 Hz, 2H), 8.19 (d, J = 8.0 Hz, 2H), 7.86 (s, 2H), 7.79 (t, J = 7.7 Hz, 2H).

4,5-diphenyl-7H-dibenzo[de,g]quinolin-7-one (A): Phenanthrene-9,10-dione (1.00 g, 4.80 mmol), NH$_4$OAc (1.08 g, 14.01 mmol), [Cp*RhCl$_2$]$_2$ (0.30 g, 0.48 mmol), Cu(OAc)$_2$·H$_2$O (4.80 g, 23.08 mmol) and 1,2-diphenylacetylene (2.22 g, 23.62 mmol) were dissolved in 120 mL of TFE. The reaction mixture was refluxed at 120 ^{o}C for 24 h under a nitrogen atmosphere. After solvent was evaporated in vacuum, the mixture was dissolved in dichloromethane, washed with water (3 × 100 mL). The organic layer was dried over anhydrous Na$_2$SO$_4$ and concentrated in vacuum. The residue was chromatographed on silica using dichloromethane/petroleum ether (1:50, v/v) as the eluent to form faint yellow solid (1.50 g, 81.43%). m.p.: > 260□. ^{1}H NMR (500 MHz, CDCl$_3$, δ): 8.56 (d, J = 7.8 Hz, 1H), 8.41 (d, J = 7.0 Hz, 1H), 8.31 (d, J = 8.0 Hz, 1H), 7.83-7.73 (m, 3H), 7.60 (t, J = 8.0 Hz, 1H), 7.47-7.45 (m, 2H), 7.41-7.39 (m, 3H), 7.30-7.28 (m, 2H), 7.25-7.21 (m, 3H). ^{13}C NMR (126 MHz, CDCl$_3$, δ): 182.40, 153.48, 145.63, 139.88, 136.98, 136.61, 135.69, 135.01, 133.84, 131.70, 131.12, 130.64, 130.61, 129.10, 128.94, 128.49, 128.31, 127.92, 127.86, 127.67, 127.56, 123.95, 123.43, 123.15. HRMS: Calcd. for C$_{28}$H$_{17}$NO, 384.1310 [M+1]; Found: 384.1387. Anal. Calcd. for C$_{28}$H$_{17}$NO: C, 87.71; H, 4.47; N, 3.65. Found: C, 87.63; H, 4.49; N, 3.68.

3,4-diphenyl-6H-phenanthro[3,4,5-$defg$]quinolin-6-one (B): The preparation of the compound **B** was similar to the compound **A**, which was obtained from the reaction between pyrene-4,5-dione (1.50 g, 6.46 mmol) and 1,2-diphenylacetylene (0.73 g, 7.77 mmol) in the presence of NH$_4$OAc (1.50 g, 19.46 mmol), Cu(OAc)$_2$·H$_2$O (3.22 g, 14.58 mmol) and

[Cp*RhCl$_2$]$_2$ (0.11g, 0.18mmol). The crude was chromatographed on silica, eluting with dichloromethane/petroleum ether (1:50, v/v) to form faint yellow solid (2.00 g, 75.99%). m.p.: > 260 □. ^{1}H NMR (500 MHz, CDCl$_3$, δ): 8.95 (d, J = 7.2 Hz, 1H), 8.36 (d, J = 8.0 Hz, 1H), 8.18 (d, J = 8.8 Hz, 1H), 8.06 (d, J =8.8 Hz, 1H), 8.01 (d, J =8.5 Hz, 1H), 7.94 (d, J = 7.5 Hz, 1H), 7.91 (d, J = 9.5 Hz, 1H), 7.50 (t, J = 7.5 Hz, 2H), 7.44 (d, J = 4.9 Hz, 3H), 7.35 (t, J = 5.2 Hz, 2H), 7.25 (t, J = 4.6 Hz, 3H). ^{13}C NMR (126 MHz, CDCl$_3$, δ): 182.90, 154.77, 146.30, 140.22, 136.72, 136.12, 135.69, 134.96, 131.56, 131.44, 131.35, 131.24, 130.73, 130.50, 130.46, 129.47, 128.38, 127.96, 127.73, 127.62, 127.47, 126.75, 126.09, 123.66, 121.50. HRMS: Calcd. for C$_{30}$H$_{17}$NO, 408.1310 [M+1]; Found: 408.1367. Anal. Calcd. for C$_{30}$H$_{17}$NO: C, 88.43; H, 4.21; N, 3.44. Found: C, 88.50; H, 4.19; N, 3.46.

2.3 Crystallography

Suitable single crystal of the compound **A** obtained from its ethyl acetate solution was selected for data collection that was performed on Bruker Smart Apex CCD diffractometer equipped with graphite-monochromatic Mo Kα radiation ($λ$ = 0.71073 Å) at 298 (2) K. Its structures were solved by direct methods and refined by full-matrix least-squares method on F^2 using SHELXL.

3. Results and discussion

3.1 Synthesis and characterization

The compound **A** and **B** were synthesized from one-pot three-component reaction of the corresponding diketone (phenanthrene-9,10-dione or pyrene-4,5-dione), ammonium acetate and 1,2-diphenylacetylene using [Cp*RhCl$_2$]$_2$ catalyst associated with the oxidant Cu(OAc)$_2$·H$_2$O in

trifluoroethanol (TFE), as shown in Scheme 1.
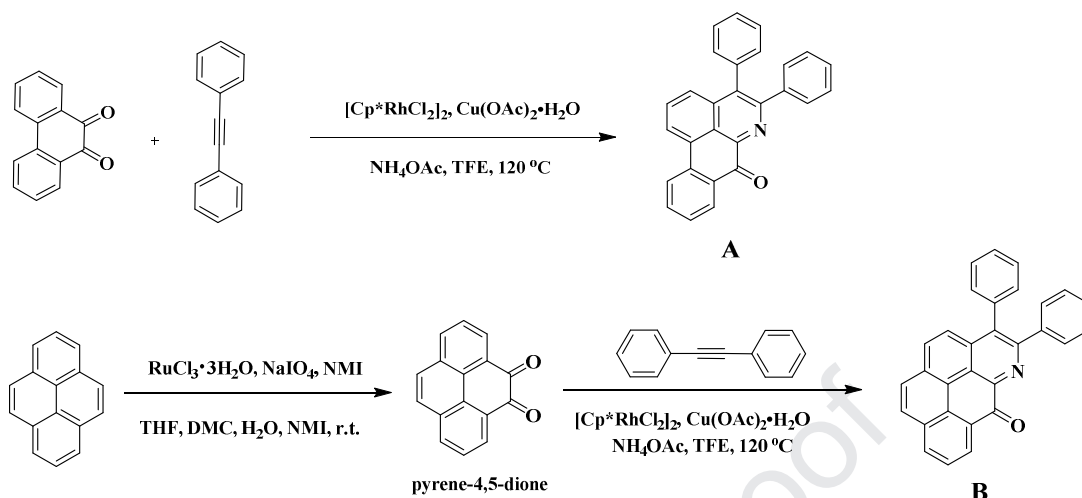
Scheme 1. Synthetic routes to the compounds **A** and **B**.
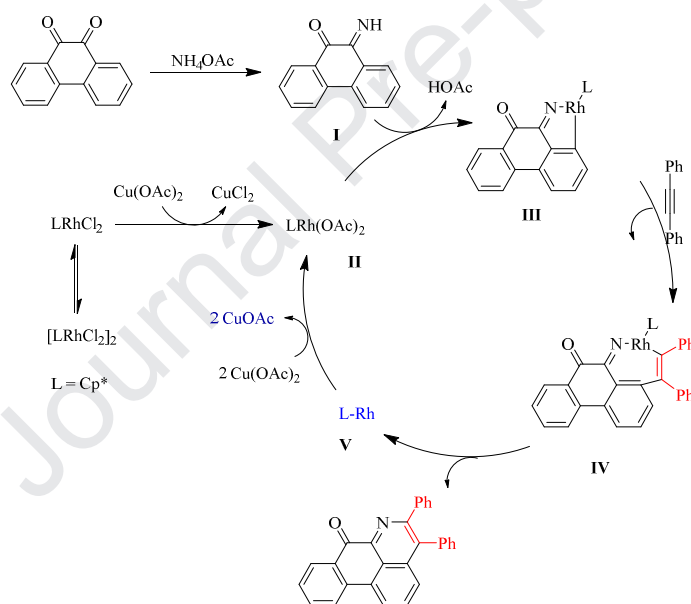
Scheme 2. The supposed reaction mechanism for the compound **A**.

Based on the previous report [45], we herein propose the rhodium (III)-catalyzed annulation

mechanism depicted in Scheme 2. Phenanthrene-9,10-dione is transferred into imine **I** readily.

Initially, the reactive Cp*Rh(OAc)$_2$ **II** is in situ generated from [Cp*RhCl$_2$]$_2$ and Cu(OAc)$_2$ via

acetate-Cl exchange. While treated with the catalyst **II**, the imine **I** undergoes the C-H and N-H

cleavages and produces five-membered cyclic Rh-intermediate **III**. Then, the intermolecular

8

insertion of the alkyne into the Rh-C bond of **III** affords the seven-membered rhodiumcyclic

intermediate **IV**. Subsequently, the intramolecular oxidative coupling of the C-N bond of **IV** and

simultaneous reductive elimination of L-Rh **V** from Rh(III) to Rh(0) releases the

isoquinoline-nucleated aromatic cyclic product. Finally, the catalyst Cp*Rh(OAc)$_2$ **II** is

regenerated via re-oxidation of Rh(0) intermediate **V** by Cu(OAc)$_2$.

The compound **A** and **B** were purified by chromatography to yield pure solid products, and

characterized using ^{1}H NMR, ^{13}C NMR and high resolution mass spectra. In addition, the

molecular structure of the compound **A** was further confirmed by X-ray crystallography.

The crystal structure of the compound **A** is shown in Fig. 1. The crystal of the compound **I**

belongs to the monoclinic space group *P2(1)/c*, a = 13.2489(11) Å, b = 8.4596(8) Å, c =

18.1875(15) Å, $\alpha = \gamma = 90^o$, $\beta = 103.057(2)^o$, U = 1985.8(3) Å^3, Z = 4, D_c = 1.283 g cm^{-3}, μ =

0.077 mm^{-1}. As shown in Fig. 1, the dibenzo[de,g]quinolin-7-one framework is nearly on a plane,

and the dihedral angles between dibenzo[de,g]quinolin-7-one skeleton and the two propeller-like

benzene rings are 51.94^o and 60.71^o, respectively. The dihedral angle between the two benzene

rings in the propeller-like diphenylethylene moiety is 49.97^o.
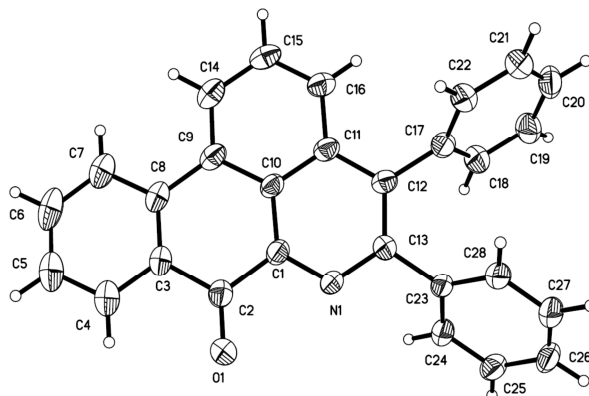

Fig. 1. Crystal structure of the compound **A**.

3.2 Thermal properties of the compounds

The thermal stabilities of the compound **A** and **B** were investigated by thermal gravimetric

analysis (TGA) measurements in nitrogen atmosphere, and the TGA curves of the compounds are given in Fig. 2. The compounds showed good thermal stability up to 360 $^{\circ}$C (< 2% weight loss), and the thermal decomposition temperature of the compound **B** (396 $^{\circ}$C) is higher than that of the compound **A** (369 $^{\circ}$C). From their molecular structures, the conjugation and size of the polycyclic aromatic skeleton of the compound **B** is larger than that of the compound **A**, the π-π interaction of the polycyclic aromatic skeleton between the compound **B** molecules should be stronger, thus the thermal stability of the compound **B** is better than that of the compound **A**. Their thermal decomposition temperatures are over than 360 °C, these compounds are suitable for the fabrication of OLED devices by evaporation.
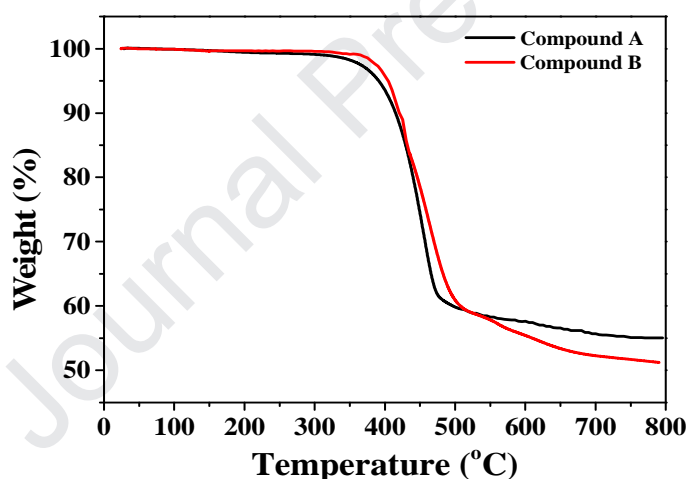

Fig. 2. Thermogravimetric analyses (TGA) of the compound **A** and **B** in nitrogen atmosphere (heating rate: 10 °C/min).

3.3 Photophysical and electrochemical properties of the compounds

The UV–vis absorption and photoluminescence (PL) spectra of the compounds in dichloromethane solutions are shown in Fig. 3, and their photophysical data are summarized in Table 1.

As shown in Fig. 3, the compound **A** exhibited three absorption bands at 253, 324 and 418 nm, respectively, which could be attributed to $\pi \rightarrow \pi^*$ transition of the polycyclic aromatic skeleton.

Compound with the compound **A**, the absorption bands of the compound **B** were red-shifted and three absorption bands were located at 257, 325 and 427 nm due to the extended π-conjugation caused by the aromatic ring expansion of the polycyclic aromatic skeleton. This spectral redshift also occurs in their photoluminescence spectra, it is found that the compound **A** and **B** exhibited green emission with peaks at 510 and 537 nm, respectively. The absolute photoluminescence quantum yields (Φ_f) of the compound **A** and **B** in dichloromethane solutions (ca. 10^{-6} mol/L) were measured to be 5.30% and 6.20% at room temperature, and their photoluminescence decay lifetimes were measured to be 23.44 and 9.75 ns. The decay profiles monitored at the respective emission maximum wavelengths are given in Fig. 4.
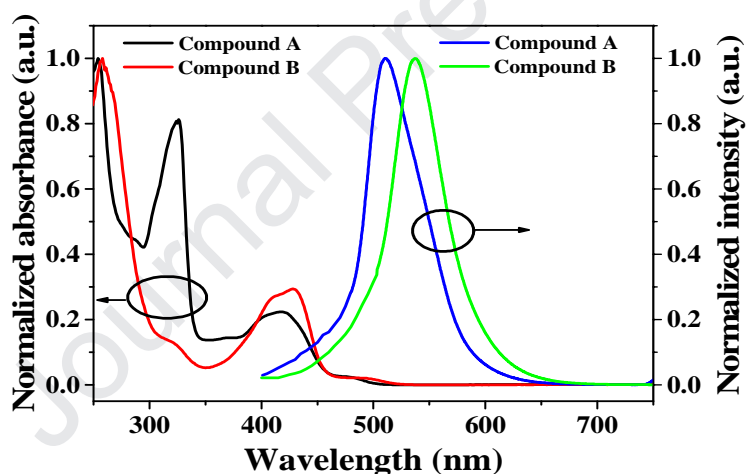

Fig. 3. UV–vis absorption and photoluminescence spectra of the compound **A** and **B** in dichloromethane solutions (C = 1.0×10^{-5} mol/L).

From the photoluminescence quantum yields (Φ_f) and the photoluminescence decay lifetimes (τ) of the compound **A** and **B**, the radiative rate constants (k_r) and nonradiative rate constants (k_{nr}) of the compound **A** and **B** were approximately calculated according to the equations [46]: $k_r = \Phi_f/\tau$ and $k_{nr} = (1-\Phi_f)/\tau$, assuming that $\Phi_{ISC} = 1$ (ISC = intersystem crossing). The radiative rate constants of the compound **A** and **B** were calculated to be 2.26×10^6 and 6.36×10^6 s^{-1}, and their nonradiative rate constants were calculated to be 4.04×10^7 and 9.62×10^7 s^{-1}, respectively.
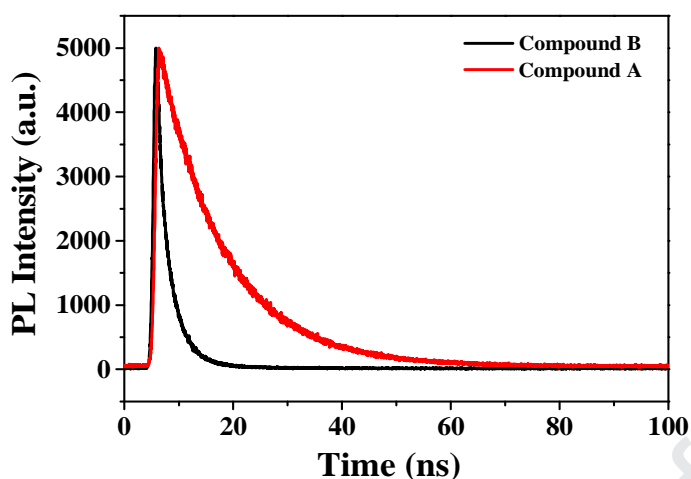
11

Fig. 4. Photoluminescence decay lifetimes of the compounds in dichloromethane solutions at room temperature (C = 1.0×10^{-6} mol/L).
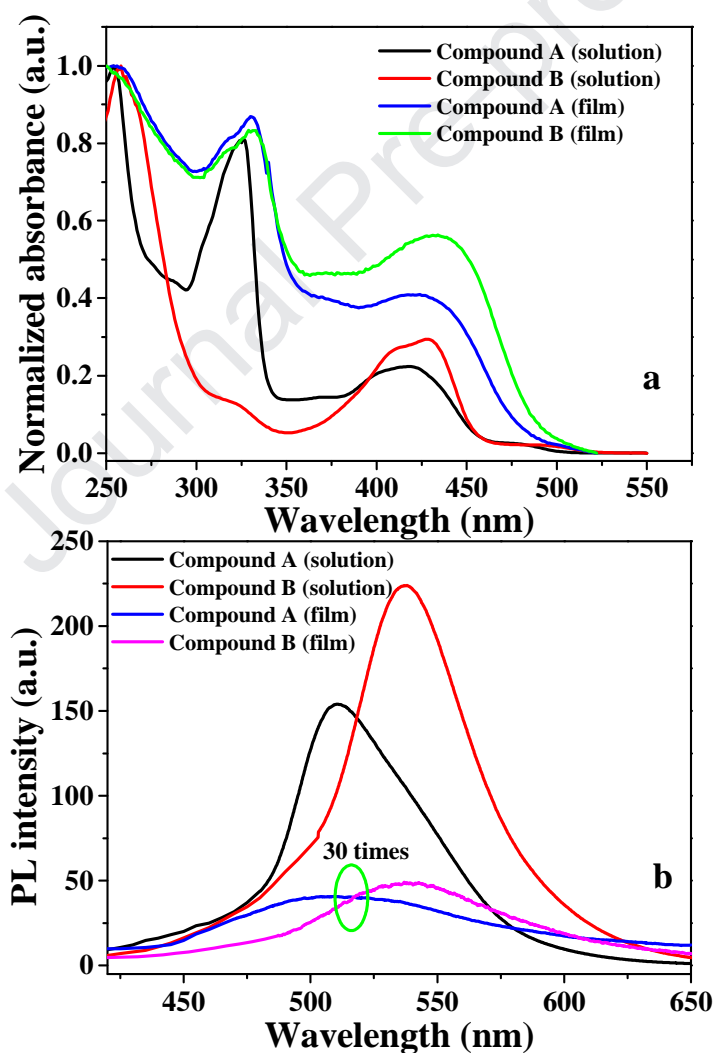

Fig. 5. The contrast diagrams of UV–vis absorption (a) and photoluminescence spectra (b) of the compound A and B in dichloromethane solutions (C = 1.0×10^{-5} mol/L) and in the solid films.

In order to compare the UV-vis absorption and photoluminescence spectra of the compounds in the solutions and solid films, Fig. 5 shows the constrast diagrams of UV–vis absorption and photoluminescence spectra of the compounds in two states of existence. From Fig. 5(a), the absorption spectra of the compounds in the solid films are similar to those in the solutions, but their absorption spectra in the solid films shift red. However, the fluorescence quenching of the compounds is very serious in the solid films, and the emissions of the compounds in the solid films are very weak (Fig. 5(b)). When the PL intensities were magnified 30 times, their emission bands in the solid films could be observed (emission peaks at 511 and 538 nm), which strongly resemble those in the solutions.

Additionally, it was found that these two compounds exhibited a certain aggregation-induced emission (AIE) phenomenon. Both compounds are soluble in many common organic solvents such as tetrahydrofuran, chloroform, toluene, acetonitrile and acetone, slightly soluble in methanol, and insoluble in water. To determine whether the compound **A** and **B** possess AIE behaviors, their fluorescent behaviors were investigated in acetone/water mixture solvent with different water fractions (f_w, vol%) (C = 1.0×10^{-4} mol/L). As shown in Fig. 6(a), in dilute acetone solution, the compound **A** was almost non-emissive under excitation at 418 nm. Afterwards, the photoluminescence intensity of the compound **A** gradually increased with increasing the content of water, and its emission spectrum also shifted slightly to longer wavelength region. When the content of water (f_w) reached to 50% in acetone/water, the photoluminescence intensity of the compound **A** reached the maximum value (ca. 1192), which was about 80-fold higher than that in acetone. When f_w was over 50%, the fluorescence intensity tended to decrease gradually. The emission intensity of the compound **A** in acetone/water with f_w of 90% was about 15.8-fold higher

13

than that in acetone. The compound **B** also exhibited a fluorescent behavior similar to that of the compound **A** with the increase of the content of water in acetone/water mixed solvent, but its fluorescent change was not as obvious as that of the compound **A**. As shown in Fig. 6(b), the compound **B** displayed weak blue emission with peak at 470 nm in dilute acetone solution, and with increasing the content of water, its photoluminescence intensity gradually increased and its emission spectrum obviously red-shifted. As f_w is 40%, the acetone-water mixture's photoluminescence of the compound **B** enhanced the maximum value and the PL intensity was approximately 3 times higher than that in acetone, and its emission peak was shifted to 508 nm. When f_w was over 40%, the PL intensity of the compound **B** gradually decreased, and even when f_w was over 70%, its PL intensity was weaker than that in acetone.

In dilute acetone solutions, two phenyl blades on the polycyclic aromatic skeletons of the compound **A** and **B** rotate around the single-bond axles linking the peripheral aryl rotors, and the intramolecular rotation converts photonic energy to heat and deactivates the excited states non-radiatively, leading to the molecules non-emissive or weak emissive [33]. When the poor solvent water was added, the solutions of the compounds gradually changed viscous, and the intramolecular rotations of the compounds were restricted and the non-radiative relaxation channel was obstructed, leading to the PL enhancement of the compounds. However, f_w was over 50% for the compound **A** and 40% for the compound **B**, the π–π stacking interaction in the viscous solutions of the compounds increased, which caused the formation of aggregates and leaded PL quenching of the compounds. The photoluminescence of the compound **A** and **B** in solid states were checked with a hand-held UV lamp, both of them really exhibited very weak blue-green emission. It is indicated that the compound **A** and **B** have aggregation-caused quenching
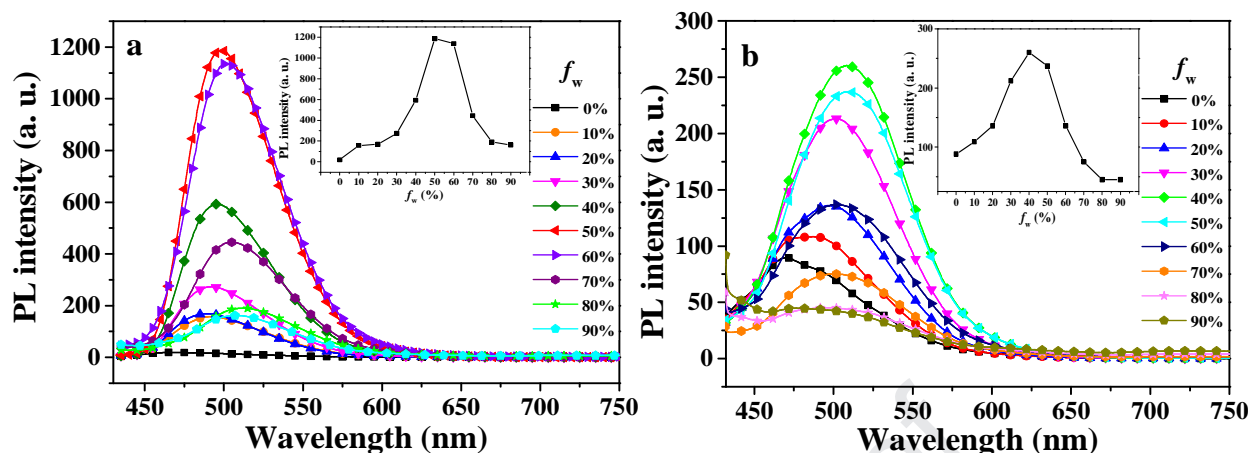
14

characteristics.

Fig. 6. PL spectra and intensities (inset) of the compound **A** (a) and **B** (b) in acetone/water with different water fraction f_w. (C = 1.0×10^{-4} mol/L).

From the structures of the compound **A** and **B**, as the central stators, the conjugated degree of 7*H*-dibenzo[*de*,*g*]quinolin-7-one core in the compound **A** is less than that of 6*H*-phenanthro[3,4,5-*defg*]quinolin-6-one core in the compound **B**. The energy change of 7*H*-dibenzo[*de*,*g*]quinolin-7-one core caused by the rotations of two phenyl rotors in the compound **A** is larger than that of 6*H*-phenanthro[3,4,5-*defg*]quinolin-6-one core by the rotations of two phenyl rotors in the compound **B**. Thus, the fluorescent change of the compound **A** is more obvious with the increase of the content of water in acetone/water mixed solvent.

The electrochemical properties of the compounds were investigated by cyclic voltammetry (CV). The cyclic voltammograms of the compound **A** and **B** are shown in Fig. 7, the first oxidation potentials of the compound **A** and **B** were located at 1.23 and 0.98 V, respectively. At the same condition, the Fc/Fc$^+$ potential was measured to be 0.54 V. The HOMO energy levels of the compound **A** and **B** were found to be -5.49 and -5.24 eV as calculated from their initial oxidation potentials [47]. From the absorption spectra in in dichloromethane solutions, the optical band edges of the compound **A** and **B** were estimated to be at *ca*. 457 nm, the optical bandgaps of these

compounds were calculated to be 2.72 eV. Thus, the LUMO energy levels of the compound **A** and

B were calculated to be -2.77 and -2.52 eV, respectively.

The photophysical, electrochemical and thermal properties of the compound **A** and **B** are
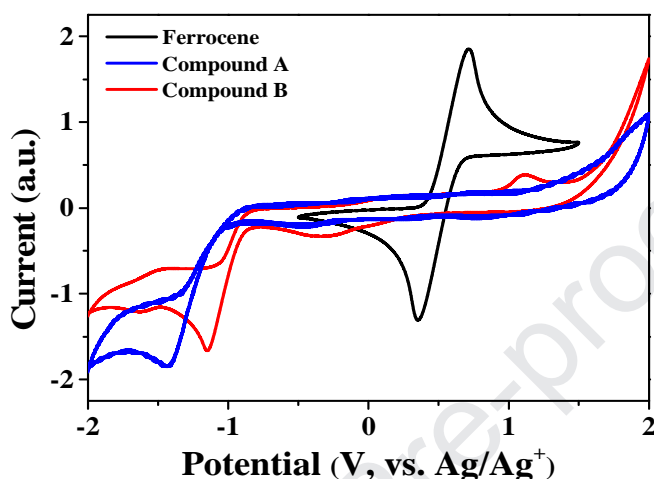
summarized in Table 1.

Fig. 7. Cyclic voltammograms of ferrocene and the compound **A** and **B** (scan rate: 10 mV/s; solvent: dichloromethane).

Table 1. Photophysical, thermal and electrochemical properties of the compound **A** and **B**

Compound	UV-vis (nm)	PL (nm)	T_d (^{o}C)	Φ_f (%)	τ (ns)	k_r/k_{nr} ($\times 10^6$ s^{-1})[a]	E_{OX} (V)[b]	E_{opt} (eV)[c]	HOMO (eV)[d]	LUMO (eV)[e]
A	253, 324, 418	510	369	5.30	23.44	2.26/40.40	1.23	2.72	-5.49	-2.77
B	257, 325, 427	537	396	6.20	9.75	6.36/96.21	0.98	2.72	-5.24	-2.52

[a]k_r and k_{nr} calculated by using the equations: $k_r = \Phi_f/\tau$ and $k_{nr} = (1-\Phi_f)/\tau$, assuming that $\Phi_{ISC} = 1$ (ISC = intersystem crossing);
[b]All the values are referred to Ag/AgCl and calibrated by Fc/Fc$^+$;
[c]$E_{opt} \approx 1241/\lambda_{onset}$;   [d]$E_{HOMO} = -e(E_{OX} - 0.51 + 4.8)$ (eV);   [e]$E_{LUMO} = E_{opt} + E_{HOMO}$

Based on the X-ray data of the compound **A**, the structures of the compounds were optimized

by density functional theory (DFT) using a CAM-B3LYP/6-31+G* basis set to calculate the

frontier molecular orbitals of the compounds. The electronic distributions of the HOMO and

16

LUMO orbitals for the compounds obtained from time-dependent DFT (TD-DFT) calculation are depicted in Fig. 8. In the HOMO orbitals of the compound **A** and **B**, the electron densities distribute not only on the isoquinoline-nucleated polycyclic aromatic skeletons, but also on two propeller-like benzene rings. However, in the LUMO orbitals of the compound **A** and **B**, all the electron densities completely locate on the isoquinoline-nucleated polycyclic aromatic skeletons, and there are no electron densities on two propeller-like benzene rings. From the electronic distributions of HOMO and LUMO orbitals of the compound **A** and **B**, their UV-vis absorption bands can be attributed to the charge transfer type π–π* transitions from the HOMO located at two propeller-like benzene rings to the LUMO located at the isoquinoline-nucleated polycyclic aromatic moieties.
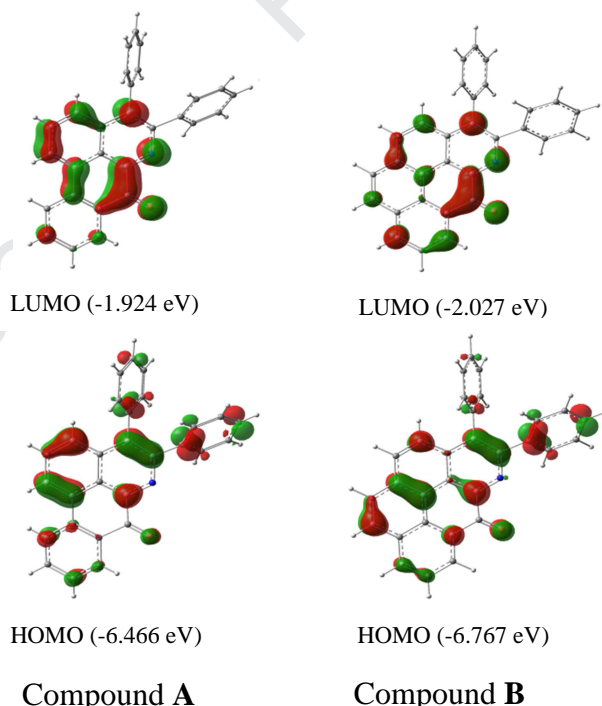

LUMO (-1.924 eV)   LUMO (-2.027 eV)

HOMO (-6.466 eV)   HOMO (-6.767 eV)

Compound **A**   Compound **B**

Fig. 8 Frontier orbitals of the compound **A** and **B** calculated at the DFT CAM-B3LYP/6-31+G* level of theory.

3.4 Electroluminescence properties of the compounds

The multilayer OLEDs with a device structure of ITO/TAPC (30 nm)/TBADN:Dopant (x

17

wt%, 30 nm)/TPBi (30 nm)/Liq (2 nm)/Al (100 nm) were fabricated by vacuum-processed method

as previously described [41], in which the compound **A** and **B** were the dopants. The device

configuration and the energy level diagrams of the materials used in the work are shown in Fig. 9.

The device performances (EL spectra, *J-V* curves, EQE values) were recorded with a Spectra

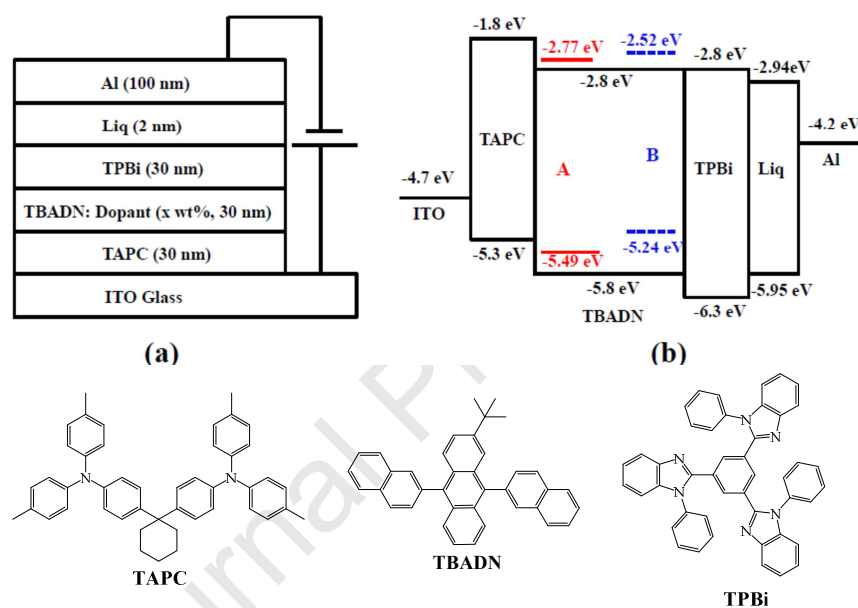Scan PR655 and a computer controlled Keithley 2400 Sourcemeter.

Fig. 9. Schematic diagram of the OLED device configuration (upper left), the relative HOMO/LUMO energy levels of the materials investigated in this work (upper right) and structures of TAPC, TBADN and TPBi (bottom).

The current density-voltage-luminance (*J–V–L*) curves and the current efficiency-power

efficiency-luminance (*CE–L–PE*) curves of the devices based on the compound **A** and **B** are

illustrated in Fig. 10 and Fig. 11, and their EL performances are summarized in Table 2. It was

shown that obvious concentration quenching effects was found with increasing from 7 wt% to 13

wt% for the compound **A** and from 4 wt% to 13 wt% for the compound **B**. The devices fabricated

from the compound **A** at 7 wt% doping concentration can approach maximum brightness of 1035

cd/m^2 at 13 V and a maximum current efficiency of 1.20 cd/A, and corresponding to a power

efficiency of 0.47 lm/W and a maximum external quantum efficiency (EQE) of 0.89% were obtained. For the compound **B**, the device with 4 wt% doping concentration exhibited maximum brightness of 2162 cd/m^2 at 12 V, but the device with 7 wt% doping concentration showed a maximum current efficiency of 2.97 cd/A, maximum power efficiency of 1.40 lm/W and maximum EQE of 2.23%. By comparing the device performances of the compounds, it can be seen that the compound **B** exhibited better EL performances than the compound **A**, which could be attributed to its higher photoluminescence quantum yield, consistent with the results of the experiments.
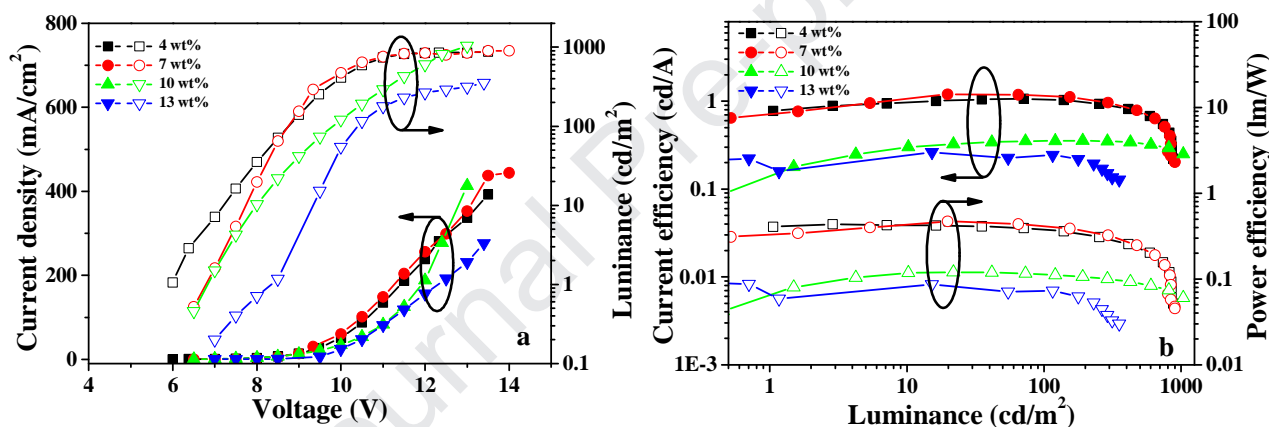

Fig. 10. *L–I–V* characteristics (a) and *CE–L–PE* curves (b) of the devices based on the compound **A** with different dopant concentrations.
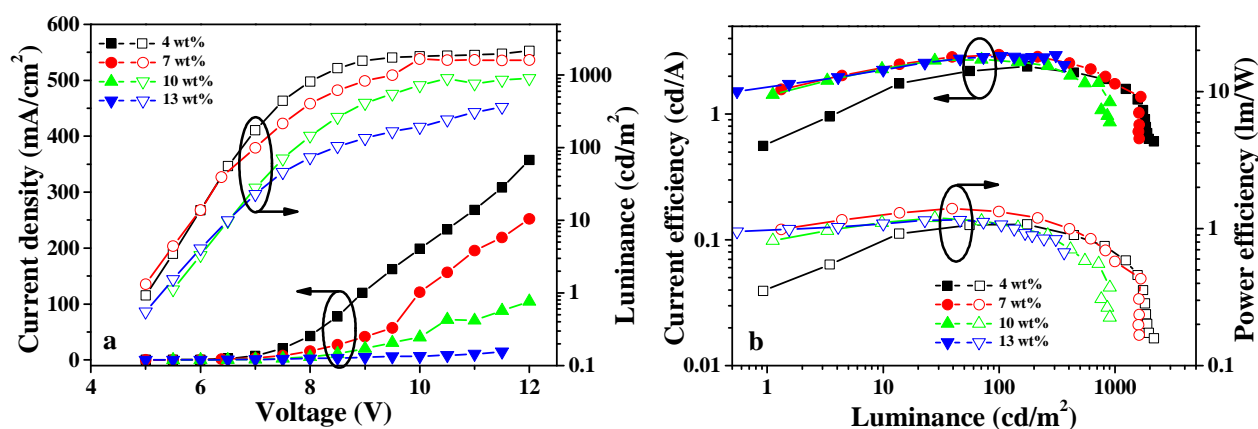

Fig. 11. *L–I–V* characteristics (a) and *CE–L–PE* curves (b) of the devices based on the compound **B** with different dopant concentrations.

19

Table 2. EL performances of the compound **A** and **B**

Compound	Concentration	EL_{max} (nm)	L_{max} (cd/m^2)	LE_{max} (cd/A)	PE_{max} (lm/W)	EQE_{max} (%)
A	4 wt%	510	873	1.06	0.44	0.79
	7 wt%	510	1035	1.20	0.47	0.89
	10 wt%	510	899	0.36	0.11	0.27
	13 wt%	511	353	0.24	0.09	0.17
B	4 wt%	537	2162	2.39	1.07	1.93
	7 wt%	537	1664	2.97	1.40	2.23
	10 wt%	538	901	2.72	1.20	1.70
	13 wt%	538	364	2.70	1.16	1.53

4. Conclusions

Two new isoquinoline-nucleated polycyclic aromatics (compound **A** and **B**) were synthesized via one-pot three-component reaction of the corresponding diketone (phenanthrene-9,10-dione or pyrene-4,5-dione), ammonium acetate and 1,2-diphenylacetylene using [Cp*RhCl$_2$]$_2$ catalyst associated with the oxidant Cu(OAc)$_2$·H$_2$O. Both compounds emit very weak fluorescence in acetone, but their luminescence intensity increased gradually when the water content (f_w) was from 0 to 50%, exhibiting aggregation-induced emission (AIE) characteristics. However, f_w was over 50% for the compound **A** and 40% for the compound **B**, their PL intensities decreased due to the formation of aggregates by π–π stacking interaction in the viscous solutions of the compounds. These compounds have good thermal stability, and the vacuum-processed doped devices were fabricated. The EL performance of devices based on the compound **B** was higher than that of the devices fabricated from the compound **A**, which could be attributed to its higher photoluminescence quantum yield. The device with the compound **B** (4 wt%) exhibited a maximum brightness of 2162 cd/m^2, and the device with 7 wt% of the compound **B** showed a maximum current efficiency of 2.97 cd/A and a maximum external quantum efficiency (EQE) of

2.23%.

Acknowledgements

Supplementary material

CCDC 1936905 contains the supplementary crystallographic data for the compound **A** in this paper. The data can be obtained free of charge via http:www.ccdc.cam.ac.uk/conts/retrieving.html, or from the Cambridge Crystallographic Data Centre, 12 Union Road, Cambridge CB2 1EZ, UK; fax: (+44) 1223-336-033; or e-mail: deposit@ccdc.cam.ac.uk.

References

[1] M.D. Watson, A. Fechtenkötter, K. Müllen, Big is beautiful-"aromaticity" revisited from the viewpoint of macromolecular and supramolecular benzene chemistry, Chem. Rev. 2001, 101, 1267-1300.

[2] A. Mishra, P. Buerle, Small molecule organic semiconductors on the move: Promises for future solar energy technology, Angew. Chem. Int. Ed., 2012, 51, 2020-2067.

[3] T. Itoh, Fluorescence and phosphorescence from higher excited states of organic molecules, Chem. Rev., 2012, 112, 4541-4568.

[4] S.R. Forrest, M.E. Thompson, Eds. Chem. Rev., 2007, 107, 923-1386 (Special issue on Organic Electronics and Optoelectronics).

[5] A.M. van de Craats, J.M. Warman, A. Fechtenkötter, J.D. Brand, M.A. Harbison, K. Müllen,

Record charge carrier mobility in a room-temperature discotic liquid-crystalline derivative of hexabenzocoronene, Adv. Mater., 1999, 11, 1469-1472.

[6] A.M. van de Craats, N. Stutzmann, O. Bunk, M.M. Nielsen, M. Watson, K. Müllen, H.D. Chanzy, H. Sirringhaus, R.H. Friend, Meso-epitaxial solution-growth of self-organizing discotic liquid-crystalline semiconductors, Adv. Mater., 2003, 15, 495-499.

[7] T.M.Figueira-Duarte, K. Müllen, Pyrene-based materials for organic electronics, Chem. Rev., 2011, 111, 7260-7314.

[8] X. Feng, J.-Y. Hu, F. Iwanaga, N. Seto, C. Redshaw, M. R. J. Elsegood, T. Yamato, Blue-emitting butterfly-shaped 1,3,5,9-tetraarylpyrenes: Synthesis, crystal structures, and photophysical properties, Org. Lett., 2013, 15, 1318-1321.

[9] Y. Niko, S. Kawauchi, S. Otsu, K. Tokumaru, G.-i. Konishi, Fluorescence enhancement of pyrene chromophores induced by alkyl groups through σ–π conjugation: Systematic synthesis of primary, secondary, and tertiary alkylated pyrenes at the 1, 3, 6, and 8 positions and their photophysical properties, J. Org. Chem. 2013, 78, 3196-3207.

[10] M.Z.K. Baig, B. Prusti, D. Roy, P.K. Sahu, M. Sarkar, A. Sharma, M. Chakravarty, Weak donor-/strong acceptor-linked anthracenyl π☐conjugates as solvato(fluoro)chromophore and AEEgens: Contrast between nitro and cyano functionality, ACS Omega, 2018, 3, 9114-9125.

[11] T. Kojima, I. Kawajiri, J. Nishida, C. Kitamura, H. Kurata, M. Tanaka, H. Ikeda, T. Kawase, 2,3-Diphenylphenanthro[9,10-b]furan derivatives as new blue fluorophores, Bull. Chem. Soc. Jpn., 2016, 89, 931-940.

[12] T.Z. Yu, X.Y. Li, Y.L. Zhao, Q.G. Yang, Y.M. Li, H. Zhang, Z.L. Li, Phenanthro[9′,10′:4,5]imidazo[2,1-*a*]isoquinoline derivatives containing phenoxazine moiety:

Synthesis and photophysical properties, J. Photochem. Photobiol. A: Chem., 2018, 360, 58-63.

[13] U.H.F. Bunz, The larger linear N☐heteroacenes, Acc. Chem. Res., 2015, 48, 1676-1686.

[14] J.-S. Wu, S.-W. Cheng, Y.-J. Cheng, C.-S. Hsu, Donor–acceptor conjugated polymers based on multifused ladder-type arenes for organic solar cells, Chem. Soc. Rev., 2015, 44, 1113-1154.

[15] W.Z. Zhang, F. Zhang, R.Z. Tang, Y.B. Fu, X.Y. Wang, X.D. Zhuang, G.F. He, X.L. Feng, Angular BN-heteroacenes with *syn*-structure-induced promising properties as host materials of blue organic light-emitting diodes, Org. Lett., 2016, 18, 3618-3621.

[16] J.E. Anthony, Functionalized acenes and heteroacenes for organic electronics, Chem. Rev., 2006, 106, 5028-5048.

[17] B.W. Yang, P.D.Q. Dao, N.S. Yoon, C.S. Cho, Copper-catalyzed C-C coupling and cyclization: Synthesis of benzo[4,5]imidazo[1,2-*a*]pyridines and benzo[4,5]imidazo[2,1-a]isoquinolines, J. Organomet. Chem., 2017, 851, 136-142.

[18] S.Q. Zhang, Z.Q. Liu, Q. Fang, Synthesis, structures, and optoelectronic properties of pyrene-fused thioxanthenes, Org. Lett., 2017, 19, 1382-1385.

[19] W.-Q. Miao, J.-Q. Liu, X.-S. Wang, An efficient synthesis of 6-arylbenzo[4,5]imidazo[2,1-*a*]isoquinolines via sequential α-arylation of carbonyl and deacylation catalyzed by CuI, Org. Biomol. Chem., 2017, 15, 5325-5331.

[20] K. Skonieczny, J. Yoo, J.M. Larsen, E.M. Espinoza, M. Barbasiewicz, V.I. Vullev, C.-H. Lee, D.T. Gryko, How to reach intense luminescence for compounds capable of excited-state intramolecular proton transfer? Chem. Eur. J., 2016, 22, 7485-7496.

[21] S. Karthik, J. Ajantha, C.M. Nagaraja, S. Easwaramoorthi, T. Gandhi, Synthesis and

photophysics of extended π-conjugated systems of substituted 10-aryl-pyrenoimidazoles, Org. Biomol. Chem., 2016, 14, 10255-10266.

[22] V.P. Boyarskiy, D.S. Ryabukhin, N.A. Bokach, A.V. Vasilyev, Alkenylation of Arenes and Heteroarenes with Alkynes, Chem. Rev., 2016, 116, 5894-5986.

[23] T. Eicher and S. Hauptmann (eds), The Chemistry of Heterocycles, Wiley-VCH Verlag GmbH, Weinheim, 2003.

[24] S.R. Neufeldt, M.S. Sanford, Controlling site selectivity in palladium-catalyzed C–H bond functionalization, Acc. Chem. Res., 2012, 45, 936-946.

[25] G.Y. Song, F. Wang, X.W. Li, C–C, C–O and C–N bond formation via rhodium(III)-catalyzed oxidative C–H activation, Chem. Soc. Rev., 2012,41, 3651-3678.

[26] L. Ackermann, Carboxylate-assisted ruthenium-catalyzed alkyne annulations by C–H/Het–H bond functionalizations, Acc Chem. Res., 2014, 47, 281-295.

[27] S. Murai, F. Kakiuchi, S. Sekine, Y. Tanaka, A. Kamatani, M. Sonoda, N. Chatani, Efficient catalytic addition of aromatic carbon-hydrogen bonds to olefins, Nature, 1993, 366, 529-531.

[28] T. Satoh, M. Miura, Oxidative coupling of aromatic substrates with alkynes and alkenes under rhodium catalysis, Chem. Eur. J., 2010, 16, 11212-11222.

[29] W. Wang, J.-L. Niu, W.-B. Liu, T.-H. Shi, X.-Q. Hao, M.-P. Song, Rhodium(III)-catalyzed annulation of 2-arylimidazo[1,2-*a*]pyridines and alkynes via direct double C–H activation, Tetrahedron, 2015, 71, 8200-8207.

[30] L.Y. Zheng, R.M. Hua, Modular assembly of ring-fused and π□extended phenanthroimidazoles via C–H activation and alkyne annulation, J. Org. Chem., 2014, 79, 3930-3936.

[31] Th. Förster, K. Kasper, Ein Konzentrationsumschlag der Fluoreszenz, Z. Phys. Chem. (Munich), 1954, 1, 275-277.

[32] S.W. Thomas, G.D. Joly, T.M. Swager, Chemical sensors based on amplifying fluorescent conjugated polymers, Chem. Rev., 2007, 107, 1339-1386.

[33] Z.F. Fei, N. Kocher, C.J. Mohrschladt, H. Ihmels, D. Stalke, Single crystals of the disubstituted anthracene 9,10-$(Ph_2P=S)_2C_{14}H_8$ selectively and reversibly detect toluene by solid-state fluorescence emission, Angew. Chem. Int. Ed., 2003, 42, 783-787.

[34] P. Chikhaliwala, S. Chandra, Dendrimers: New tool for enhancement of electrochemiluminescent signal, J. Organomet. Chem., 2016, 821, 78-90.

[35] P.L. Burn, S.-C. Lo, I.D.W. Samuel, The development of light-emitting dendrimers for displays, Adv. Mater., 2007, 19, 1675-1688.

[36] J.D. Luo, Z.L. Xie, J.W.Y. Lam, L. Cheng, H.Y. Chen, C.F. Qiu, H.S. Kwok, X.W. Zhan, Y.Q. Liu, D.B. Zhu, B.Z. Tang, Aggregation-induced emission of 1-methyl-1,2,3,4,5-pentaphenylsilole, Chem. Commun., 2001, 1740-1741.

[37] B.Z. Tang, X.W. Zhan, G. Yu, P.P.S. Lee, Y.Q. Liu, D.B. Zhu, Efficient blue emission from siloles, J. Mater. Chem., 2001, 11, 2974-2978.

[38] Z.J. Ning, Z. Chen, Q. Zhang, Y.L. Yan, S.X. Qian, Y. Cao, H. Tian, Aggregation-induced emission (AIE)-active starburst triarylamine fluorophores as potential non-doped red emitters for organic light-emitting diodes and Cl_2 gas chemodosimeter, Adv. Funct. Mater., 2007, 17, 3799-3807.

[39] Y.N. Hong, J.W.Y. Lam, B.Z. Tang, Aggregation-induced emission: phenomenon, mechanism and applications, Chem. Commun., 2009, 4332-4353.

[40] Y.N. Hong, J.W.Y. Lam, B.Z. Tang, Aggregation-induced emission, Chem. Soc. Rev., 2011, 40, 5361-5388.

[41] J. Mei, N.L.C. Leung, R.T.K. Kwok, J.W.Y. Lam, B.Z. Tang, Aggregation-Induced Emission: Together We Shine, United We Soar! Chem. Rev., 2015, 115, 11718-11940.

[42] Z.J. Zhao, B.R. He, B.Z. Tang, Aggregation-induced emission of siloles, Chem. Sci., 2015, 6, 5347-5365.

[43] J. Mei, Y.N. Hong, J.W.Y. Lam, A.N.J. Qin, Y.H. Tang, B.Z. Tang, Aggregation-induced emission: The whole is more brilliant than the parts, Adv. Mater., 2014, 26, 5429-5479.

[44] J.C. Walsh, K.-L. M. Williams, D. Lungerich, G.J. Bodwell, Synthesis of pyrene-4,5-dione on a 15 g scale, Eur. J. Org. Chem., 2016, 5933-5936.

[45] L. Ackermann, Carboxylate-assisted ruthenium-catalyzed alkyne annulations by C–H/Het–H bond functionalizations, Acc Chem. Res., 2014, 47, 281-295.

[46] Z.R. Hao, M. Li, Y.J. Liu, Y.F. Wang, G.H. Xie, Y. Liu, Near-infrared emission of dinuclear iridium complexes with hole/electron transporting bridging and their monomer in solutionprocessed organic light-emitting diodes, Dyes and Pigments, 2018, 149, 315-322.

[47] T.Z. Yu, Z.Y. Zhu, Y.J. Bao, Y.L. Zhao, X.X. Liu, H. Zhang, Investigation of novel carbazole-functionalized coumarin derivatives as organic luminescent materials, Dyes and Pigments, 2017, 147, 260-269.

Research Highlights

1. Two isoquinoline-nucleated polycyclic aromatic compounds were synthesized via one-pot three-component reaction.

2. They exhibited aggregation-induced emission (AIE) characteristics when the water content (f_w) was from 0 to 50%.

3. The device based on 3,4-diphenyl-6H-phenanthro[3,4,5-$defg$]quinolin-6-one displayed the brightness of 2162 cd/m^2 and luminous efficiencies of 2.97 cd/A, and EQE of 2.23%.